VIROLOGY

Human intestinal tract serves as an alternative infection route for Middle East respiratory syndrome coronavirus

Jie Zhou,[1,2,3]* Cun Li,[2]* Guangyu Zhao,[4]* Hin Chu,[1,2,3] Dong Wang,[2] Helen Hoi-Ning Yan,[5] Vincent Kwok-Man Poon,[2] Lei Wen,[2] Bosco Ho-Yin Wong,[2] Xiaoyu Zhao,[2] Man Chun Chiu,[2] Dong Yang,[2] Yixin Wang,[2] Rex K. H. Au-Yeung,[5] Ivy Hau-Yee Chan,[6] Shihui Sun,[4] Jasper Fuk-Woo Chan,[1,2,3,7,8] Kelvin Kai-Wang To,[1,2,3,7,8] Ziad A. Memish,[9,10] Victor M. Corman,[11,12] Christian Drosten,[11,12] Ivan Fan-Ngai Hung,[13] Yusen Zhou,[4†] Suet Yi Leung,[5] Kwok-Yung Yuen[1,2,3,7,8†‡]

Middle East respiratory syndrome coronavirus (MERS-CoV) has caused human respiratory infections with a high case fatality rate since 2012. However, the mode of virus transmission is not well understood. The findings of epidemiological and virological studies prompted us to hypothesize that the human gastrointestinal tract could serve as an alternative route to acquire MERS-CoV infection. We demonstrated that human primary intestinal epithelial cells, small intestine explants, and intestinal organoids were highly susceptible to MERS-CoV and can sustain robust viral replication. We also identified the evidence of enteric MERS-CoV infection in the stool specimen of a clinical patient. MERS-CoV was considerably resistant to fed-state gastrointestinal fluids but less tolerant to highly acidic fasted-state gastric fluid. In polarized Caco-2 cells cultured in Transwell inserts, apical MERS-CoV inoculation was more effective in establishing infection than basolateral inoculation. Notably, direct intragastric inoculation of MERS-CoV caused a lethal infection in human DPP4 transgenic mice. Histological examination revealed MERS-CoV enteric infection in all inoculated mice, as shown by the presence of virus-positive cells, progressive inflammation, and epithelial degeneration in small intestines, which were exaggerated in the mice pretreated with the proton pump inhibitor pantoprazole. With the progression of the enteric infection, inflammation, virus-positive cells, and live viruses emerged in the lung tissues, indicating the development of sequential respiratory infection. Taken together, these data suggest that the human intestinal tract may serve as an alternative infection route for MERS-CoV.

INTRODUCTION

Middle East respiratory syndrome coronavirus (MERS-CoV) was identified as a novel zoonotic virus causing human respiratory infection in 2012 (*1*). As of July 2017, MERS-CoV has caused 2037 laboratory-confirmed infection cases, including 710 deaths, with a crude case fatality rate of about 35% (*2*). The clinical spectrum of MERS ranged from asymptomatic or mild respiratory disease to acute fulminant pneumonia with respiratory distress syndrome or multiorgan failure resulting in a fatal outcome. Common symptoms were fever, cough, and shortness of breath. Gastrointestinal symptoms were among the most commonly reported extrapulmonary clinical features of MERS; about one-third of MERS patients had gastrointestinal tract symptoms such as abdominal pain, nausea, vomiting, and diarrhea (*3*, *4*).

It has been reported that up to 20% of MERS cases are considered as primary infections due to contact with camels (*5*). MERS-CoV–infected camels, especially the juvenile ones, were found to shed a large amount of the virus from the upper respiratory tract (*6*). Camel milk may also play a role in the transmission of MERS-CoV. MERS-CoV could be detected in 41.7% of milk samples collected from lactating camels, which also actively shed the virus in nasal secretion and/or feces (*7*). In addition, MERS-CoV can survive in camel milk for a prolonged period (*8*). The consumption of unpasteurized camel milk was found to be a source of infection in some MERS patients (*9*). Thus, it is generally believed that primary infection, that is, MERS-CoV transmission from camel to human, is mediated via respiratory droplet and/or saliva during direct contact with camels or through consumption of camel milk or undercooked camel meat (*10*).

Meanwhile, a large proportion of MERS cases occurred in healthcare settings, in which respiratory droplets of MERS patients as well as direct or indirect contact have been postulated to be important for virus transmission (*3*, *11*). Theoretically, human-to-human virus transmission mediated by respiratory droplets (>5 μm in size) occurs within 1 to 2 m from a source patient. However, history of direct contact can be inferred in only about 10% of patients in the largest hospital-associated MERS outbreak reported so far, which occurred in the Republic of Korea, with 186 infection cases in 2015 (*12*). Most of the cases in this large-scale outbreak were those who shared the same healthcare environment without direct contact with MERS patients. Therefore, fomite transmission may explain a significant proportion of the infections (*12*). The virological evidence to support fomite transmission is that MERS-CoV remains stable at low temperatures and

[1]State Key Laboratory of Emerging Infectious Diseases, University of Hong Kong, Hong Kong, China. [2]Department of Microbiology, University of Hong Kong, Queen Mary Hospital, Pokfulam, Hong Kong, China. [3]Research Centre of Infection and Immunology, University of Hong Kong, Hong Kong, China. [4]State Key Laboratory of Pathogen and Biosecurity, Beijing Institute of Microbiology and Epidemiology, Beijing, China. [5]Department of Pathology, University of Hong Kong, Queen Mary Hospital, Pokfulam, Hong Kong, China. [6]Department of Surgery, Queen Mary Hospital, Hong Kong, China. [7]Carol Yu Centre for Infection, University of Hong Kong, Hong Kong, China. [8]Collaborative Innovation Center for Diagnosis and Treatment of Infectious Diseases, University of Hong Kong, Hong Kong, China. [9]Ministry of Health and College of Medicine, Alfaisal University, Riyadh, Kingdom of Saudi Arabia. [10]Hubert Department of Global Health, Rollins School of Public Health, Emory University, Atlanta, GA 30322, USA. [11]Institute of Virology, Charité–Universitätsmedizin Berlin, Berlin, Germany. [12]German Centre for Infection Research (DZIF), Berlin, Germany. [13]Department of Medicine, University of Hong Kong, Queen Mary Hospital, Hong Kong, China.
*These authors contributed equally to this work.
†These authors contributed equally to this work.
‡Corresponding author. Email: kyyuen@hku.hk

low humidity, and could be recovered after exposure to the environment for 48 hours (*13*). Accordingly, viral RNA can be extensively detected in the environmental surfaces in rooms of MERS patients (*14*). Given that fomite transmission may play a role in the outbreak in healthcare settings, acquisition of MERS-CoV infection via the gastrointestinal tract should be seriously considered. Collectively, in both camel-to-human transmission and human-to-human transmission, there is a possibility that humans may acquire MERS-CoV infection upon exposure to the virus through the gastrointestinal tract.

A protein intrinsic disorder–based model was previously established to classify transmission behaviors of coronaviruses by measuring the percentage of intrinsic disorder in the two major shell (matrix and nucleocapsid) proteins of coronaviruses (*15*). The analysis of protein sequences of these two proteins of MERS-CoV suggests that MERS-CoV belongs to a category of coronaviruses that have relatively hard inner and outer shells; therefore, it may persist in the environment for a prolonged period and may have an oral-fecal transmission ability (*16*). The bioinformatically predicted MERS-CoV survival upon environmental exposure has been experimentally corroborated (*13*). Here, we sought to elucidate whether the gastrointestinal tract could be an alternative infection route for MERS-CoV and whether the exposure of MERS-CoV to the gastrointestinal tract can subsequently lead to a respiratory infection. To this end, we performed in vitro studies in human primary intestinal epithelial cells, intestinal explants, polarized Caco-2 cells, and human intestinal organoids, as well as an in vivo study in human dipeptidyl peptidase 4 (hDPP4) transgenic mice.

RESULTS

Susceptibility of human primary intestinal epithelial cells and small intestine explants to MERS-CoV, and evidence of alimentary infection in clinical MERS patients

To address whether the human gastrointestinal tract could serve as an infection route for MERS-CoV, we examined the susceptibility of human primary intestinal epithelial cells to MERS-CoV. To this end, human primary intestinal epithelial cells were cultured for 1 week for differentiation. The differentiated epithelial cells were inoculated with MERS-CoV and were fixed at 24 hours post-infection (hpi) for immunofluorescence staining to identify the virus-positive cell. Almost all the inoculated intestinal epithelial cells highly expressed MERS-CoV NP, whereas no viral protein was detectable in mock-infected cells (Fig. 1A). In addition, the infected cells underwent significant membrane fusion and formed syncytia. Consistent with the intensive expression of viral protein, the viral load increased by more than 1 log in the MERS-CoV–inoculated epithelial cells (fig. S1). To further verify the infectivity of MERS-CoV in human intestinal epithelium, normal human small intestine from a surgical resection was obtained with informed consent and used for MERS-CoV inoculation. Despite tissue degradation, immunofluorescence staining explicitly revealed NP-positive enterocytes in the infected intestine (Fig. 1B) at 20 hpi. The infected enterocytes formed syncytia similar to those in the primary cells. Although only patchy areas of epithelium were infected, we observed an increased viral load of about 1 log in the Matrigel and medium, as well as in the infected explants (Fig. 1C). Thus, human primary intestinal epithelial cells and small intestine can be infected by MERS-CoV and support viral replication.

In an earlier study, we reported that 12 of 82 stool specimens of MERS patients were positive for MERS-CoV RNA (*17*), suggesting the possible MERS-CoV infection in the gastrointestinal tract of these patients. To gather more evidence doe alimentary infection in MERS patients, these positive specimens were analyzed with a quantitative reverse transcription polymerase chain reaction (RT-qPCR) assay for the detection of subgenomic RNA (sgRNA) of the nucleocapsid (N) gene, an intermediate in the replication cycle of MERS-CoV. Notably, N sgRNA was detected in the specimen and was confirmed by sequencing the qPCR product, which showed a typical sgRNA sequence with fused leader sequence, the predicted transcription regulatory site (TRS), and the body element of N gene (Fig. 1D). The presence of N sgRNA in the stool specimen suggested that MERS-CoV probably infected and replicated in the alimentary tract of the MERS patient. Together, the results in human primary intestinal epithelial cells and small intestine explants, together with the examination of the MERS patient's specimen, indicated that MERS-CoV can infect and replicate in human intestinal epithelium.

Highly productive MERS-CoV infection in human intestinal organoids

Generation of intestinal organoids from $LGR5^+$ tissue-resident adult stem cells in human intestines has been a major breakthrough in the past years. The differentiated intestinal organoids harbor all types of epithelial cells in human intestine and can simulate most morphological and functional properties of in vivo tissues (*18*). Therefore, three-dimensional cultured intestinal organoids, also known as intestinoids or mini-gut, have been used to model human diseases (*19*), including the infection of enteric viruses and bacteria (*20*, *21*).

We characterized MERS-CoV infectivity and replication kinetics in human intestinoids. At 48 hours after inoculation, viral loads increased by about 3 log units in the intestinoids and in the Matrigel and medium (Fig. 2A) after inoculation with a multiplicity of infection (MOI) of 1. The infected intestinoids developed progressive cytopathic effects over time. Thus, normalized viral loads in the infected intestinoids exhibited a constant increment within the 48-hour observation window (Fig. 2B). Accordingly, plaque assays revealed a significantly increased viral titer of 3 log units in the Matrigel and medium at 48 hpi (Fig. 2C). The infection efficiency of MERS-CoV in intestinoids, that is, the percentage of MERS-CoV–infected intestinal epithelial cells, was also examined with flow cytometry. At 2 hpi, about 5% of the cells within the intestinoids were MERS-CoV NP–positive. The percentage of NP-positive cells significantly increased to approximately 25% at 24 hpi (Fig. 2, D and E), suggesting a productive virus infection and spread in the intestinoids. The productive MERS-CoV infection in intestinoids was also evidenced by a strong signal of viral NP in the virus-inoculated intestinoids, albeit absent in the mock-infected organoids (Fig. 2F). In addition, we verified the expression of the MERS-CoV receptor DPP4, a major determinant for tissue tropism of MERS-CoV, in intestinal epithelial cells by immunofluorescence staining (fig. S2). Together, human intestinal organoids were highly susceptible to MERS-CoV and supported robust viral replication.

Viability of MERS-CoV in gastrointestinal fluids

The ability to retain viability in gastrointestinal fluids is a prerequisite for a microbe to establish infection in the human alimentary tract. In this regard, we assessed whether MERS-CoV can maintain infectivity in simulated human gastrointestinal fluids. As shown in Fig. 3, MERS-CoV rapidly lost most of the infectivity in fasted-state simulated gastric fluid (FaSSGF; pH 2.0). We assume that, in a real-life scenario, the virus is more likely to be exposed to fed-state gastrointestinal fluids because it is supposed to access the stomach during food intake. Thus,

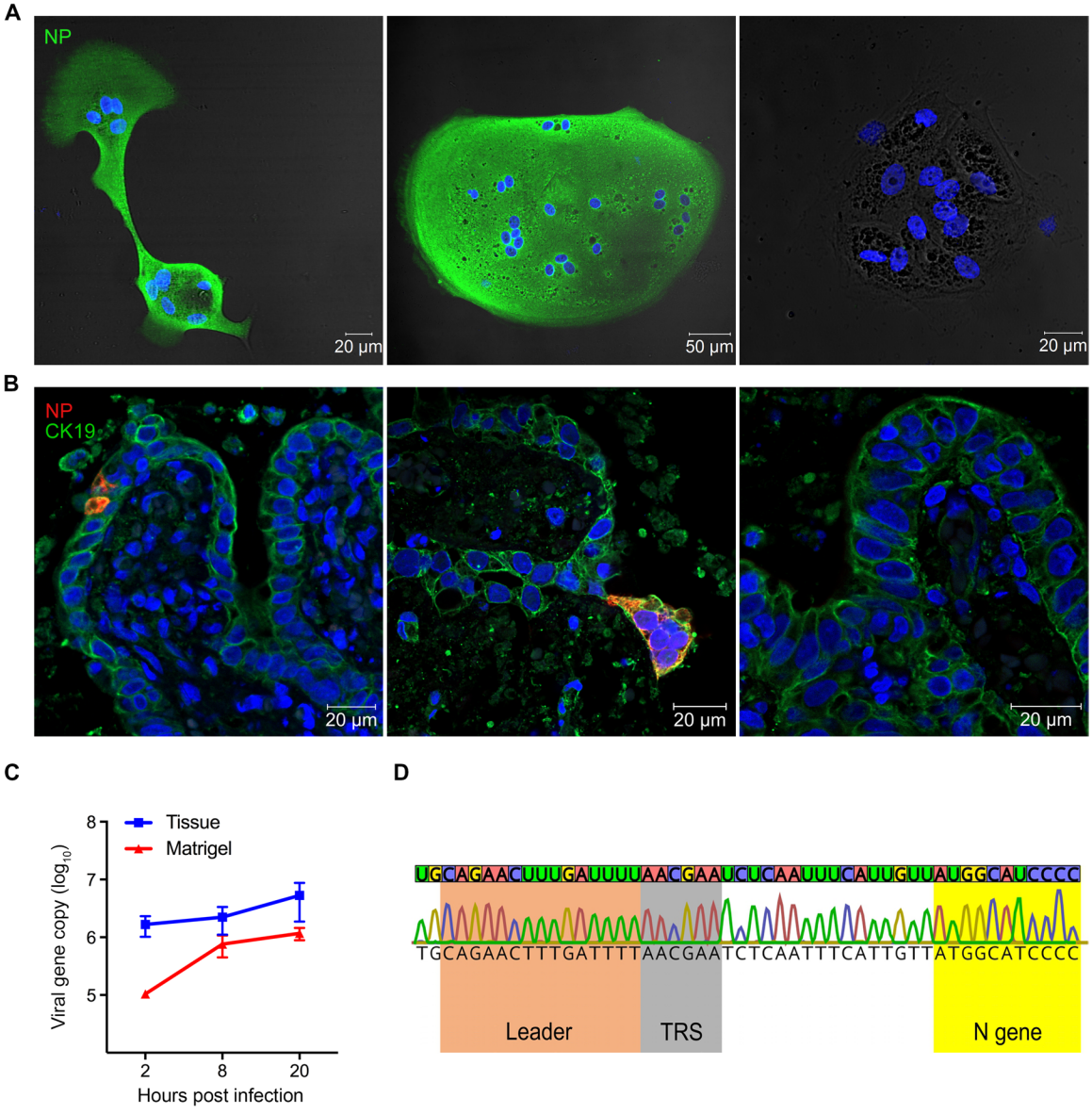

Fig. 1. Susceptibility of human primary intestinal cells, intestine explants to MERS-CoV, and identification of the replication intermediate in the stool specimen of a MERS patient. (**A**) Human primary intestinal cells were inoculated with MERS-CoV (left and middle) or mock-infected (right). At 24 hpi, cells were fixed and applied to immunofluorescence staining of MERS-CoV nucleocapsid protein (NP). Nuclei were counterstained with 4′,6-diamidino-2-phenylindole (blue). The images show the representative results of one experiment. (**B** and **C**) Normal human small intestine explants were inoculated with MERS-CoV, as described in Materials and Methods. The data show representative results of the experiments independently performed twice. (B) The infected (left and middle) and mock-infected (right) explants were fixed at 20 hpi for immunofluorescence staining of MERS-CoV NP and the enterocyte marker CK19. Syncytia formation can be observed in the infected intestinal epithelium (middle). (C) At the indicated hpi, the explants (Tissue) and Matrigel together with culture medium (Matrigel) were harvested for the quantification of viral load. Data are means ± SD of viral loads in duplicated samples. (**D**) Chromatograph of the N gene sgRNA recovered from the stool specimen of a MERS patient show fusion of leader sequence, TRS, and N gene element.

we tested the infectivity of MERS-CoV after exposure to fed-state simulated gastric fluid (FeSSGF) or fed-state simulated intestinal fluid (FeSSIF), which contains a high concentration of bile salts that solubilize the lipid membrane of enveloped viruses. The results showed that MERS-CoV survived FeSSGF while being less tolerant to FeSSIF. Nevertheless, a small proportion of the virus can survive FeSSIF after treatment for 2 hours. As a control, EV71, a prototype human enterovirus, was generally resistant to all the tested gastrointestinal fluids. Another human coronavirus, hCoV-229E, which often causes mild respiratory infection, showed a comparable sensitivity to FaSSGF and FeSSGF to MERS-CoV, but was much less resistant to the intestinal fluid than MERS-CoV. All viruses exhibited considerable stability in Dulbecco's modified Eagle's medium (DMEM) over a period of 2 hours. Collectively, MERS-CoV was able to resist, to some extent, the digestive enzymes and bile salts in the human gastrointestinal tract, although the virus was less tolerant to the high acidity of fasted-state gastric fluid.

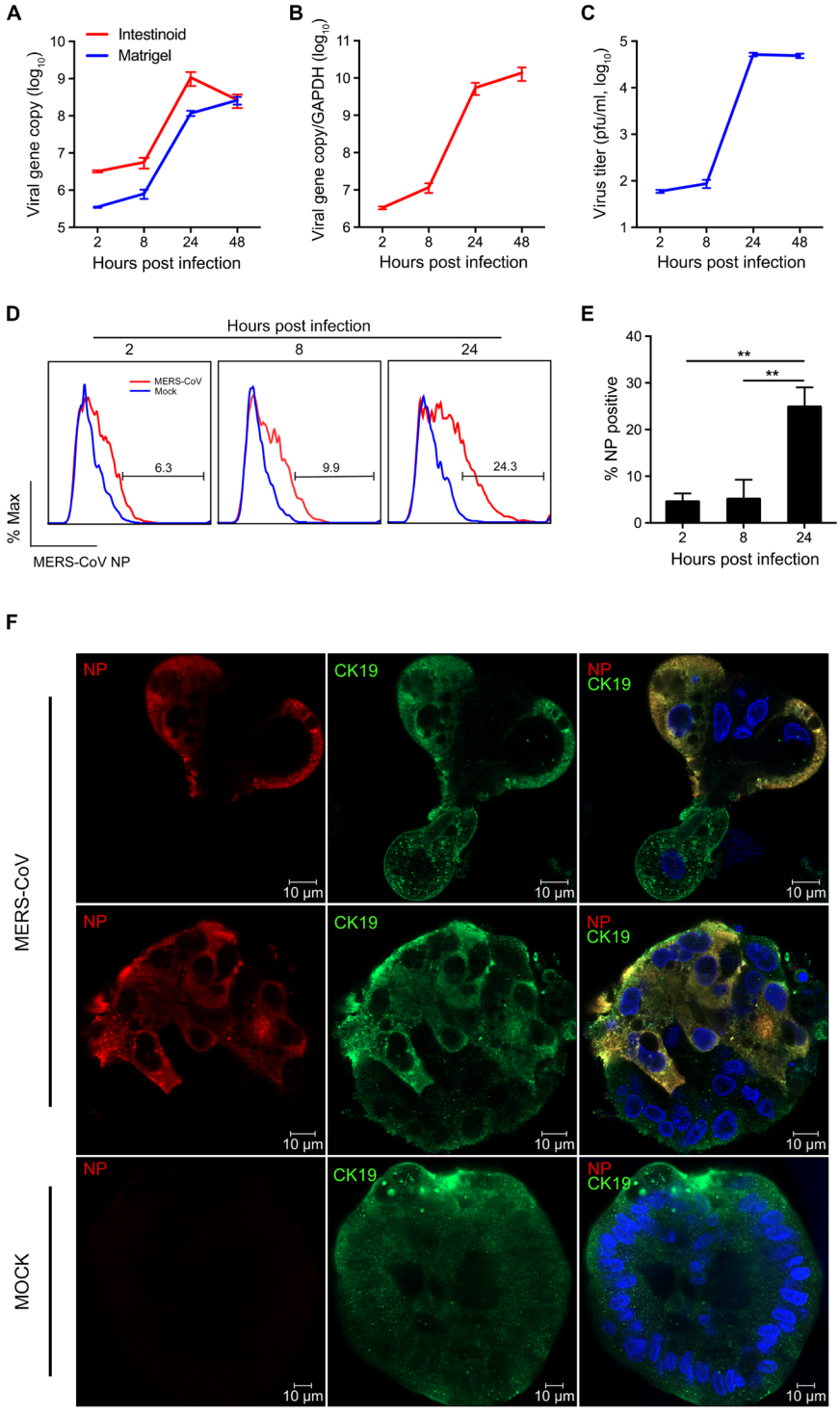

Fig. 2. MERS-CoV infection and replication in human intestinal organoids. The differentiated intestinoids were inoculated with MERS-CoV (MOI ≈ 0.05) in duplicate and then re-embedded in Matrigel and maintained in culture medium. (**A**) At the indicated hpi, intestinoids (Intestinoid), cell-free Matrigel, and culture medium (Matrigel) were harvested for the quantification of viral load with RT-qPCR. Serially diluted MERS-CoV NP plasmids were used to generate a standard curve for the quantification. (**B**) The absolute viral loads in intestinoids were normalized with GAPDH (glyceraldehyde-3-phosphate dehydrogenase) mRNA transcripts. (**C**) The dissolved Matrigel and culture medium were applied to viral titration with plaque assay. Data are means ± SD of one representative experiment independently repeated three times. (**D** and **E**) At 24 hpi, the infected and mock-infected intestinoids were fixed after disassociation and stained with the MERS-CoV NP antiserum and then applied to flow cytometry to evaluate the percentage of NP-positive cells. The histogram shows the results of one representative experiment. (E) Data are means and SD of three independent experiments. Student's *t* test was used for data analysis. $^{**}P \leq 0.01$. (**F**) At 24 hpi, the infected (MERS-CoV) and mock-infected intestinoids, after fixation and immunofluorescence staining of MERS-CoV NP and CK19, were whole-mounted and imaged with a confocal microscope.

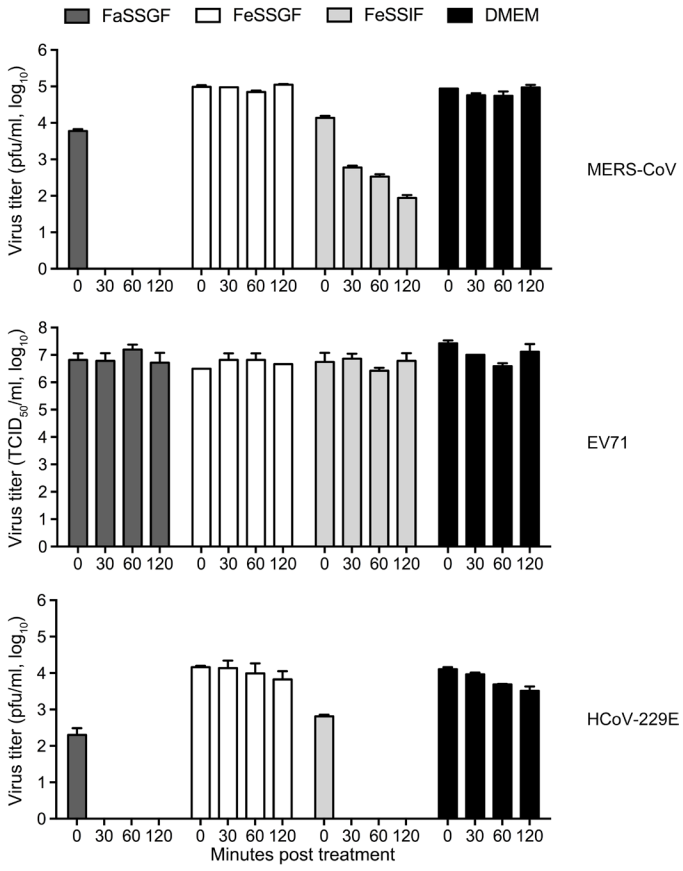

Fig. 3. MERS-CoV treatment with simulated gastrointestinal fluids. MERS-CoV solution [7.5×10^6 plaque-forming units (PFU), 500 μl] was mixed with 5 ml of FaSSGF, FeSSGF, FeSSIF, or DMEM and then incubated at 37°C for the indicated minutes. An aliquot (1 ml) of the virus/fluid mixture was sampled for virus titration in Vero-E6 cells in triplicate after neutralization with sodium hydroxide. The enterovirus EV71 and the human coronavirus hCoV-229E were treated with the same gastrointestinal fluids and titrated with $TCID_{50}$ (median tissue culture infectious dose) assay in RD cells and plaque assay in Huh7 cells, respectively. Data are from a representative experiment independently performed three times.

MERS-CoV infection and virus release in polarized intestinal epithelial cells

Caco-2 cells cultured in Transwell inserts can undergo spontaneous differentiation, display morphological and functional features of enterocytes, and form an intact permeability barrier, which could be reflected by heightened transepithelial electronic resistance (TEER), blockage of fluorescent molecule penetration, and formation of cell adhesion architecture (*22*). Thus, polarized Caco-2 cells in Transwell culture have been used to model human gastrointestinal epithelium and cellular barrier across the epithelium (*22*). We used the polarized Caco-2 cells to recapitulate the kinetics of viral growth and pattern of virus release in human intestinal epithelium after MERS-CoV inoculation.

After 2 weeks of Transwell culture, the polarized Caco-2 cells formed an intact epithelial barrier, as shown in fig. S3. The cell monolayers were then apically or basolaterally inoculated with MERS-CoV at an MOI of 0.1. Cell-free media in the upper and bottom chambers were harvested at the indicated time points for viral load quantification. Because of the formation of an intact epithelial barrier in the polarized Caco-2 cells, the viral loads detected from the media of the upper and bottom chambers can reflect the genuine pattern of virus release. As shown in Fig. 4A, after both apical and basolateral inoculation, the virus significantly replicated and bilaterally released into the media in the upper and bottom chambers. No infectious virus was detectable in the culture media at 2 hpi, whereas progeny virions were released from the apical and basolateral sides in both inoculation routes at 24 hpi (Fig. 4B). In addition, apical inoculation was more effective in establishing infection than basolateral inoculation. At 24 hours after a high MOI (2.0) inoculation, the infection rate, that is, the percentage of MERS-CoV NP–positive cells in apical inoculation, was significantly higher than that in basolateral inoculation ($P = 0.038$, Fig. 4C). Accordingly, the active caspase-3–positive cells, which underwent virus-induced apoptosis, were significantly more abundant in apical inoculation than in basolateral inoculation ($P = 0.001$). The higher infection efficiency in apical inoculation was further substantiated in immunofluorescence staining, which markedly revealed more abundant NP-positive cells via apical inoculation than basolateral inoculation (Fig. 4D). Collectively, both apical and basolateral inoculations of MERS-CoV resulted in robust viral replication in the polarized Caco-2 cells. Progeny virions were released bilaterally upon infection. Moreover, apical MERS-CoV inoculation was more effective in establishing infection than basolateral inoculation.

MERS-CoV infection in hDPP4 transgenic mice

We proceeded to evaluate whether direct intragastric MERS-CoV inoculation in the hDPP4 transgenic mouse can cause gastrointestinal infection and whether the gastrointestinal infection is followed by a respiratory infection. The hDPP4 mouse experiments were performed using our previously established mouse model of MERS-CoV infection (*23*). First, nine female mice were inoculated with 10^5 PFU of MERS-CoV via intragastric gavage; three of them were pretreated with a proton pump inhibitor, pantoprazole, to improve the viability of MERS-CoV in the mouse stomach because the in vitro experiment suggested the acid lability of MERS-CoV. At day 5 after virus inoculation, three pantoprazole-pretreated mice and three phosphate-buffered saline (PBS)–pretreated mice were sacrificed. At day 8 after inoculation, two mice lost more than 10% of their body weight and were sacrificed, whereas one mouse succumbed to the infection. Thus, direct intragastric MERS-CoV inoculation in hDPP4 mice may result in a lethal infection. To characterize the early events after intragastric MERS-CoV inoculation, nine female hDPP4 mice were inoculated via intragastric gavage; three mice were sacrificed at days 1, 3, and 5 after challenge, respectively. In addition, to exclude possible virus access to the airway during intragastric gavage, we directly injected 10^5 PFU of MERS-CoV into the stomach (intragastric injection hereafter) of 12 hDPP4 mice after a minor laparotomy. Six mice were pretreated with pantoprazole or mock-treated with PBS before the inoculation; three mice of each group were sacrificed at days 3 and 5 after inoculation.

Histopathological examination revealed that small intestines of all intragastrically inoculated mice displayed increased mononuclear cell infiltration in the lamina propria, with broadening of the intestinal villi and increased sloughing of surface epithelium. The intervening mucosa was basically normal. Figure 5A (a to c) shows the pathology of small intestines in the mice sacrificed at days 1, 3, and 5 after inoculation, respectively, indicating deteriorating inflammation and epithelial degeneration after virus inoculation. The pantoprazole-treated mice sacrificed at day 5 displayed more extensive and more prominent pathology in small intestine than the PBS-treated mice (Fig. 5A, d and e).

The mock-infected mouse showed a negligible pathological change in the intestines (Fig. 5A, f). Immunofluorescence staining was performed to identify the viral antigen (NP)–positive cell in the intestines of the inoculated mice. It was shown that intestinal epithelial cells were intensively infected at day 1 after inoculation (Fig. 5B, a to c). The infected cells were patchily distributed in the surface epithelia of small intestines (Fig. 5B, a and b). In some areas, the infected enterocytes formed syncytia (Fig. 5B, c, and fig. S4, A and B). At days 5 and 8 after inoculation, the NP-positive cells were distributed more widely in small intestines and emerged in the lamina propria (arrows in Fig. 5B, d to f) and Peyer's patch (arrowhead in Fig. 5B, d). Double staining of viral NP and CD68 revealed that some infected cells in the lamina propria were macrophages (Fig. 5B, f). Consistent with the massive inflammatory infiltration in small intestines of the inoculated mice as shown by hematoxylin and eosin (H&E) staining, CD3-positive lymphocytes were more abundant in the infected mice (Fig. 5B, a, b, and e) than those in the mock-infected mouse (Fig. 5B, h). Although there was no overt pathology in colon epithelium, NP-positive epithelial cells were nevertheless sparsely distributed in colon epithelium of infected mice (Fig. 5B, g). The viral load increased in small intestines of intragastrically injected mice, especially in the pantoprazole-pretreated mice (Fig. 5C), indicating a correlation between viral replication and intestinal pathology. However, the attempt to identify live virus from the intestine failed because the inoculation of the intestine homogenates, even the diluted homogenates, caused significant cell death and detachment of the monolayers.

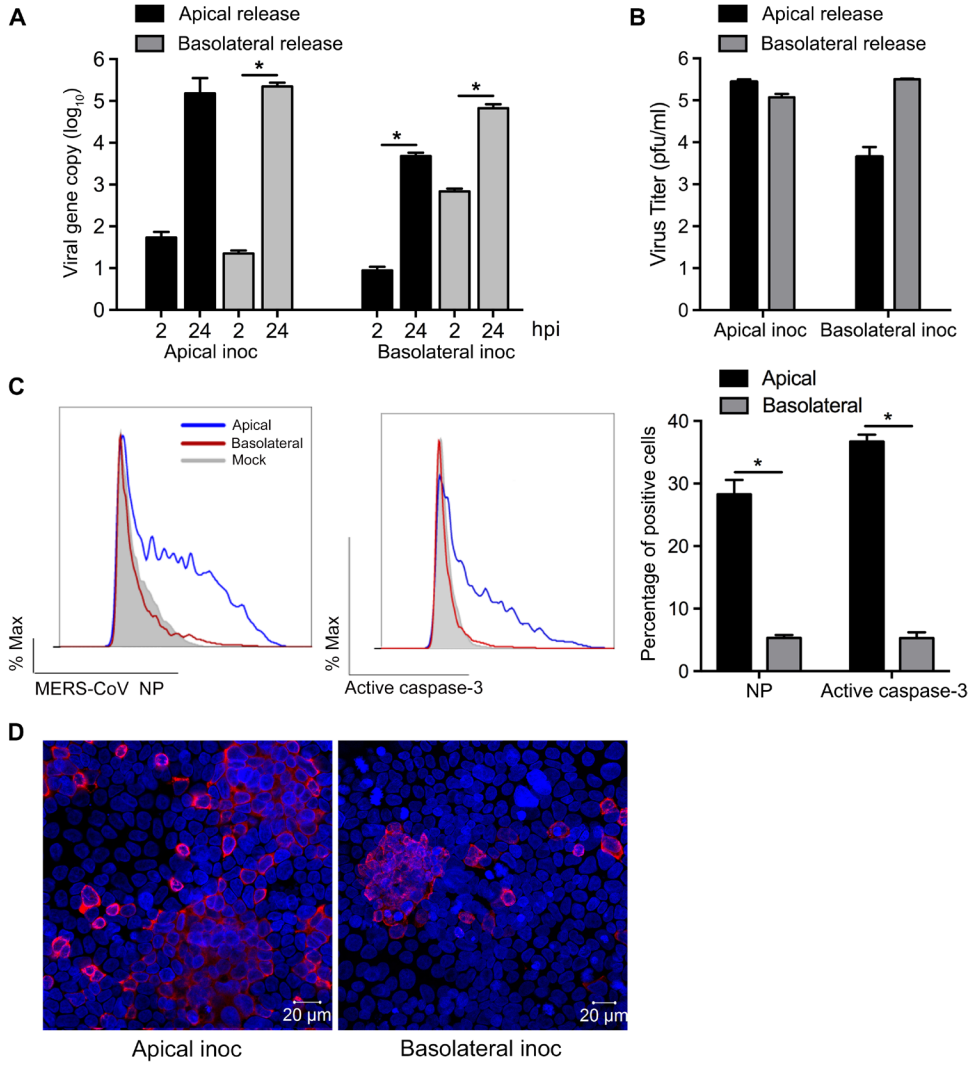

Fig. 4. MERS-CoV replication and cell apoptosis in the polarized Caco-2 cells. (**A** and **B**) The polarized Caco-2 cells were inoculated with MERS-CoV in duplicate from the apical or basolateral side of the monolayer with an MOI of 0.1. At the indicated hpi, cell-free media were harvested from the upper and bottom chambers for viral load quantification. The experiments were independently performed twice. A representative experiment is presented. (A) Viral gene copy number in the medium collected from the upper chamber (Apical release) and bottom chamber (Basolateral release) after apical inoculation (Apical inoc) and basolateral inoculation (Basolateral inoc). (B) Viral titer in the media harvested at 24 hpi detected by plaque assay. No plaque was detected in the media at 2 hpi. (**C** and **D**) The polarized Caco-2 cells were inoculated from the apical or basolateral side with MERS-CoV at an MOI of 2 or mock-inoculated. (C) At 24 hpi, cells were fixed after dissociation and applied to flow cytometry to detect the expression of MERS-CoV NP and activated caspase-3. The left and middle panels are the histograms of one representative experiment. The right panel presents means and SD of three independent experiments. *$P \leq 0.05$. (D) At 24 hpi, the polarized Caco-2 cells seeded on polycarbonate membranes were fixed and applied to immunofluorescence staining of MERS-CoV NP (red) and imaged en face.

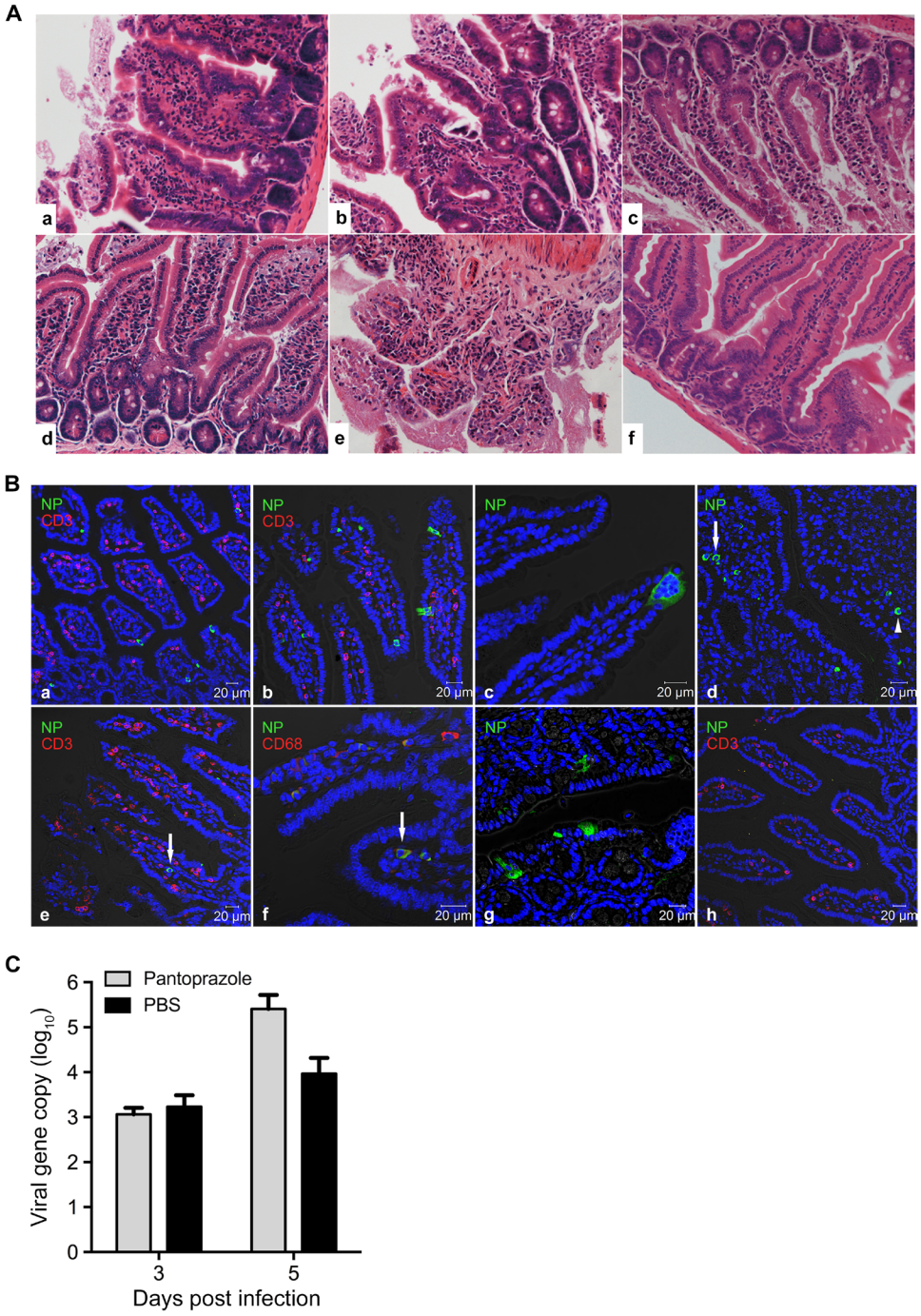

Fig. 5. MERS-CoV enteric infection in hDPP4 transgenic mice. hDPP4 mice were inoculated with MERS-CoV via direct intragastric gavage or intragastrically injected as described in Materials and Methods. (**A**) (a to c) Representative histopathology in small intestines at days 1, 3, and 5 after inoculation, respectively. (d and e) Small intestines of pantoprazole-pretreated mice at day 5 after inoculation. (f) Small intestine of a mock-infected mouse. H&E staining, magnification ×200. (**B**) Identification of MERS-CoV–infected cells in the intestines of the inoculated hDPP4 mice with immunostaining of NP and cell type markers. (a to c) Virus-positive enterocytes in mice at day 1 after inoculation. The infected enterocytes (c) form syncytia. (d to f) Virus-infected cells in mouse intestines at days 5 and 8 after inoculation, respectively. Arrows show NP-positive cells in the lamina propria, including the NP/CD68 double-positive macrophage (f). The arrowhead (in d) indicates virus-positive cells in Peyer's patch. (g) Virus-positive cells in the colon of an inoculated mouse. (h) Costaining of NP/CD3 in the mock-infected mouse. (**C**) Three intragastrically injected mice of the indicated groups were sacrificed at the indicated day after inoculation; intestine homogenates were applied for the quantification of viral load by RT-qPCR. The gray and black bars represent the viral loads of the mice pretreated with pantoprazole and mock-treated with PBS, respectively. Data are means and SD of three mice.

In the early phase up to day 5 after virus inoculation, the lung tissues of the inoculated mice showed minimal degree of inflammation (Fig. 6A, a). However, the pantoprazole-pretreated mice, which were sacrificed at the same day after inoculation, exhibited prominent pulmonary inflammation (Fig. 6A, b and c). Histological examination revealed marked infiltration of mononuclear cells and lymphocytes in the alveolar septa, indicating interstitial inflammation. Without pantoprazole pretreatment, the mice also exhibited inflammatory infiltration in the lung tissue at day 8 after intragastric gavage (Fig. 6A, d). Notably, NP-positive pneumocytes were identified in these mice (Fig. 6A, f). As expected, the abundance and distribution of virus-positive cells in the lung tissues of intragastrically inoculated mice were more limited than those in the intranasally inoculated mouse (fig. S4C). Consistent with the viral propagation in small intestines of intragastrically injected mice, viral load was elevated in the lung tissues of these mice at day 5 after inoculation, particularly in the pantoprazole-pretreated mice (Fig. 6B). Notably, infectious virions were detected in the lung homogenates of the intragastrically injected mice at day 5 after inoculation by plaque assay (fig. S5), which further verified the lung infection in these mice (Fig. 6A). We and others (*24*, *25*) observed brain infection in the intranasally inoculated hDPP4 mice. Likewise, the intragastrically injected mice also developed brain infection. Infectious virions were detected in the brain homogenates at day 5 after infection (fig. S5). The infected mice exhibited increased viral loads in the brain tissues. In summary, the direct intragastric MERS-CoV inoculation initiated an infection in the intestinal mucosa, leading to progressive inflammation and epithelial degeneration. With the progression of intestinal MERS-CoV infection, a sequential respiratory infection occurred.

DISCUSSION

The MERS epidemic has persisted for about 5 years. However, important issues related to the public health, such as mode of virus transmission and infection route, remain poorly understood. Because MERS primarily manifests as a respiratory infection, airway exposure is intuitively assumed to be the infection route, which contributes substantially to human MERS infections (*3*, *26*). Epidemiological studies, biological evaluation of the virus, and bioinformatic prediction collectively suggested that humans may also acquire MERS-CoV infection via the gastrointestinal tract. Here, we aimed to elucidate whether the gastrointestinal tract could serve as an alternative route to acquire MERS-CoV infection

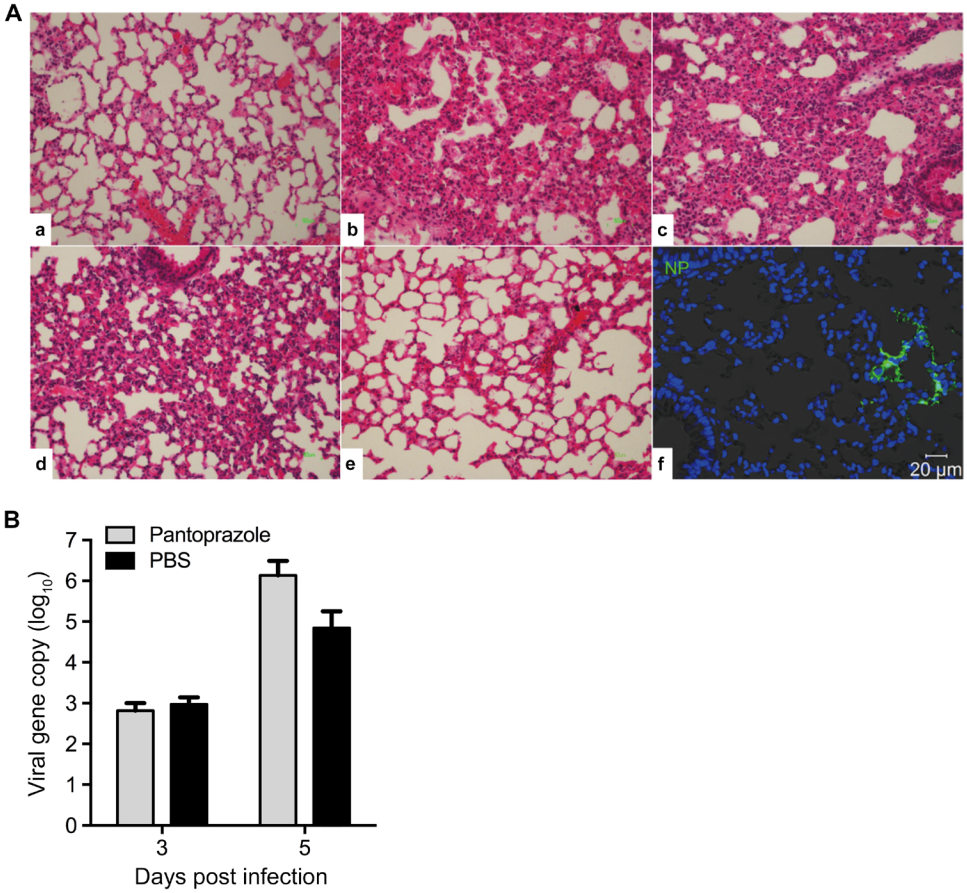

Fig. 6. Inflammation and MERS-CoV infection in the lung tissues of hDPP4 mice. (**A**) Lung tissues in the mice without pantoprazole pretreatment (a) versus those in pantoprazole pretreatment (b and c) at day 5 after intragastric MERS-CoV inoculation. (d) Lung pathology in an inoculated mouse at day 8 after intragastric inoculation without pantoprazole pretreatment. (f) Lung tissue of a mock-infected mouse. H&E staining, magnification ×200. (e) Immunostaining shows virus-positive cells (green) in the lung tissue of a mouse at day 8 after intragastric inoculation. (**B**) Lung tissues were harvested from three intragastrically injected mice at the indicated day after inoculation and homogenized for the quantification of viral load by RT-qPCR. The gray and black bars represent the viral loads of the mice pretreated with pantoprazole and mock-treated with PBS, respectively. Data are means and SD of three mice.

and whether gastrointestinal tract exposure to MERS-CoV may eventually lead to a respiratory infection.

We demonstrated that human primary intestinal epithelial cells were highly susceptible to MERS-CoV and could support viral replication (Fig. 1A). MERS-CoV infection and replication were further verified in an ex vivo culture of human small intestine (Fig. 1, B and C) and reinforced by identification of the viral replication intermediate in the stool specimen of a MERS patient (Fig. 1D). We further characterized MERS-CoV infection and replication in human intestinoids (Fig. 2), a novel ex vivo model system that can faithfully simulate the in vivo human intestinal epithelium. Notably, MERS-CoV replicated more robustly in human intestinoids than in primary respiratory epithelial cells and ex vivo lung tissues (*27*, *28*). The MERS-CoV receptor DPP4 is known as the major determinant of host and tissue tropisms in MERS-CoV (*29*). According to the public database Human Protein Atlas, human small intestine expresses the highest level of DPP4 mRNA and protein among all human organs, including lung and bronchus. Thus, the abundantly expressed DPP4 in human intestine may account for high susceptibility of these cells to MERS-CoV.

We also showed that MERS-CoV lost infectivity in highly acidic fasted-state gastric fluid, whereas it was considerably resistant to fed-state gastric fluid and intestinal fluid, which contains a large amount of digestive enzymes and bile salts (Fig. 3). It was documented that enveloped coronaviruses, unlike most enveloped viruses, are notably resistant to bile salts (*30*). Here, we verified the stability of MERS-CoV in bile salts in a very stringent setting, where the viruses were incubated with 10 volumes of FeSSIF containing a high concentration of bile salts. However, the acid instability of MERS-CoV shown in Fig. 3 seemed paradoxical, now that the intragastric inoculation of MERS-CoV caused the enteric infection in hDPP4 mice. Coincidently, an earlier study with a similar experimental setting documented the acid lability of rotavirus (*31*), a typical gastrointestinal virus that commonly causes gastroenteritis in mammals. In our study, apart from the same pH of 2.0 as in the previous study, pepsin was additionally supplemented to better simulate the authentic fasted-state gastric fluid. Thus, the lability of MERS-CoV in highly acidic FaSSGF, as shown in the in vitro assay, was probably an exaggerated result. In a real-life scenario, especially during food intake, the virus may not be exposed to such a large volume of pure gastrointestinal fluids as in the experimental setting.

MERS-CoV intestinal infection was hinted in an earlier study of intranasally inoculated hDPP4 mice (*24*), in which an increasing viral load was observed in mouse intestines after MERS-CoV inoculation. Here, we characterized MERS-CoV enteric infection in hDPP4 transgenic mice. After intragastric inoculation, the hDPP4 mice displayed viral antigen (NP)–positive cells, deteriorating inflammation, and epithelial degeneration in small intestines (Fig. 5, A and B). The viral NP-positive cells, which were distributed focally at day 1 after inoculation, became more diffuse in intestinal mucosa over time (Fig. 5B). In Transwell culture, the infected Caco-2 cells can release progeny virions apically and basolaterally (Fig. 4). Thus, it was not unexpected that NP-positive cells appeared in the lamina propria and lymphoid tissue of small intestine as the enteric infection progressed (Fig. 5B). Likewise, it is conceivable that the viruses produced in the intestinal mucosa of hDPP4 mouse may access the lymph flow and/or the bloodstream via the abundant lymphatic vessels and venules in the lamina propria of small intestine, respectively; they could be further transported to right heart via the thoracic duct and superior vena cava, and are disseminated to the lungs. The intragastrically inoculated mice exhibited minimal lung pathology at the early phase. Interstitial pneumonia occurred as the enteric infection developed; meanwhile, NP-positive cells emerged in the pulmonary parenchyma (Fig. 6A). Correspondingly, live viruses were identified in the lung homogenates of intragastrically injected mice, in which aspiration of the virus inoculum into airway was basically excluded. Consistent with the possibility of hematogenous viral trafficking, the lung tissues of intragastrically inoculated mice showed prominent interstitial pneumonia with thickened alveolar septa and mononuclear cell filtration. As frequently reported in the intranasally inoculated hDPP4 mice, brain infection also occurred in our intragastrically infected mice (fig. S5). Thus, further investigation is required to exclude the possibility that the dysfunctional brainstem due to brain infection may be attributable to the lung infection. Nevertheless, our results indicated that the MERS-CoV pulmonary infection in hDPP4 mice was secondary to the intestinal infection. Clinically, respiratory symptoms may not be the initial presentations of MERS patients (*32*, *33*). Respiratory infection as a subsequent manifestation was documented in some MERS patients, whose onset of symptoms was diarrhea and fever. In a case report, lung inflammation was an incidental finding on chest radiograph. The patient subsequently developed severe respiratory disease and died (*34*).

Virus dissemination and infection of other organs after gastrointestinal tract exposure occur in other viruses. For example, the direct intragastric inoculation of the avian influenza virus H5N1 in ferrets and hamsters caused systemic viral dissemination via the bloodstream (*35*). Human picornavirus, hepatitis A virus, enters the bloodstream after infecting human intestinal epithelium and ultimately establishes infection in the liver (*36*). Apart from the respiratory tract, the human alimentary tract is another common site for viral entry. Enteric viruses and even some non-enteric viruses can bypass the physical barriers and infect susceptible cells in the alimentary tract. To date, six human coronaviruses have been identified as the causative agents of mild or severe respiratory infections. The concomitant gastrointestinal symptoms are frequently observed in some human coronaviruses. For example, the human coronavirus OC43, which is closely related to bovine coronavirus phylogenetically, caused gastrointestinal symptoms in up to 57% of the infected patients (*37*). Notably, enteric involvement was verified in human infection of severe acute respiratory syndrome coronavirus (SARS-CoV), which caused a large-scale epidemic with more than 8000 human infections in 2002–2003 (*38*). Active SARS-CoV replication was identified in the small and large intestine specimens from colonoscopy biopsy and autopsy (*39*). A significant portion of SARS patients had gastrointestinal symptoms; the viral load was the highest in stool specimens, followed by nasopharyngeal aspiration specimens (*40*). Thus, the human gastrointestinal tract was speculated to be the primary infection site of SARS-CoV (*41*), which raised a fearsome concern of dual infectivity of SARS-CoV as being both a respiratory and gastrointestinal pathogen. However, no serious study has been reported to address the important issue. In contrast to the ambiguity of virus acquisition via the alimentary tract in human coronaviruses, it has been known that most animal coronaviruses, such as bovine coronavirus and porcine transmissible gastroenteritis virus, can primarily infect either the enteric or respiratory tract or sometimes translocate between sites (*42*, *43*). Until now, however, whether human and animal coronaviruses share similarity in terms of a dual acquisition route has remained unanswered. Here, we addressed this long-standing question in human intestinal epithelial cells, intestinal organoids, and hDPP4 transgenic mice. We demonstrate that the human intestinal tract serves as an alternative infection route for MERS-CoV. The knowledge obtained from this study will provide a scientific basis for the implementation

of effective intervention/prevention strategies to halt the continuing MERS epidemic.

MATERIALS AND METHODS

Virus infection in human primary intestinal epithelial cells, small intestine explants, intestinal organoids, and polarized Caco-2 cells

MERS-CoV of the EMC/2012 strain was provided by R. Fouchier (Erasmus Medical Center) (*1*). Clonetics normal human intestinal epithelial cells (InEpC, Lonza) were cultured in SmGM-2 Bullet medium with growth supplements. At 24 hours after MERS-CoV inoculation with an MOI of about 10, cells seeded on chamber slides were fixed with 4% paraformaldehyde and applied to immunofluorescence staining; cell-free medium and cells in a 96-well plate were harvested for the quantification of viral load with viral RNA extraction and RT-qPCR, as we described previously (*44*). Under the protocol approved by Institutional Review Board of the University of Hong Kong/Hospital Authority Hong Kong West Cluster (HKU/HA HKW IRB, UW 13-364), normal small intestine was obtained for virus inoculation from a patient who underwent surgical resection. The full-thickness tissue was excised into about 0.3 cm × 0.6 cm strips, positioned in a 12-well culture plate, and incubated with 10^7 PFU of MERS-CoV at 37°C for 2 hours. After the inoculated explants were rinsed with MEM supplemented with antibiotics, they were positioned onto Transwell inserts precoated with Matrigel. More Matrigel was applied to brace around the explants, with mucosa facing upward. The bottom chamber contained 1 ml of DMEM supplemented with six antibiotics (detailed information will be provided upon request). At the indicated hpi, the explants were harvested for the quantification of viral load and immunofluorescence staining after fixation.

Intestinal organoids derived from normal human colon were cultured, and differentiation was induced as described elsewhere (*18*). The differentiated intestinoids were mechanically sheared with Pasteur pipettes and incubated with MERS-CoV at 37°C for 2 hours with the addition of 10 μM Rho-associated coiled-coil–containing protein kinase (ROCK) inhibitor Y-27632 (STEMCELL Technologies) to inhibit spontaneous apoptosis during the inoculation. An inoculum of 10^5 PFU of MERS-CoV was used to infect one droplet of intestinoids (containing 50 to 100 intestinoids), with an estimated MOI of 0.05. After the inoculum was removed, the virus-inoculated intestinoids were rinsed with PBS and then re-embedded in Matrigel and cultured in a 24-well plate with culture medium. At the indicated hpi, the intestinoids were harvested for the quantification of viral load with RNA extraction and RT-qPCR, whereas cell-free Matrigel and culture medium were used for viral load detection and viral titration with plaque assay. In addition, infected or mock-infected intestinoids were fixed with 4% paraformaldehyde at 24 hpi, followed by immunofluorescence staining and confocal imaging. Moreover, a proportion of infected or mock-infected intestinoids, after fixation and antibody staining, were applied to flow cytometry for the examination of infection rate.

Caco-2 cells were seeded on polycarbonate inserts (0.4 μm pore size) of a 12-well Transwell plate (Corning) at a cell density of 10^5 cells/cm^2 in DMEM supplemented with 10% fetal bovine serum (FBS). Culture medium was changed every 3 days. The TEER was measured every 3 days using Millicell ERS-2 Volt-Ohm Meter (EMD Millipore). To monitor the integrity of the Caco-2 monolayer as an epithelial barrier, at the indicated day after seeding, fluorescein isothiocyanate–dextran with a molecular weight of 10 k (Sigma-Aldrich) was added in the culture medium of the upper chamber at a concentration of 1 mg/ml and incubated at 37°C for 4 hours. Subsequently, the culture media were harvested from the upper and bottom chambers to detect the fluorescence intensity using the Victor XIII Multilabel Reader (PerkinElmer). When TEER and epithelial integrity reached a plateau after 2 weeks of Transwell culture, the polarized Caco-2 cells were inoculated with MERS-CoV from the apical or basolateral side of the monolayer at an MOI of 0.1 and then maintained in DMEM without FBS. At the indicated time points after inoculation, cell-free media were harvested from the upper and bottom chambers for viral load quantification and viral titration. To examine the MERS-CoV infection efficiency in the polarized Caco-2 cells, the cells were inoculated from the apical or basolateral side with MERS-CoV at an MOI of 2 or mock-inoculated. At 24 hpi, Caco-2 monolayers were disassociated into a single-cell suspension after incubation with 0.25% trypsin-EDTA for 30 min and then fixed for flow cytometry analysis after antibody staining. The polarized Caco-2 cells seeded on polycarbonate membranes were fixed and then excited from Transwell inserts for immunofluorescence staining.

Detection of subgenomic RNA in stool specimens of MERS patients

We applied RT-PCR assays, using a leader-specific primer, and primer and probe targeting sequence downstream of the start codon of the most abundant N gene sgRNA to test whether sgRNA, the replication intermediate, is detectable in MERS-CoV RNA–positive stool specimens collected from MERS patients (*17*). Oligonucleotide sequences are as follows: MERS-sgRNA-rtF, ACTTCCCCTCGTTCTCTTGCAG; MERS-sgRNA-rtP, FAM-CACGAGCTGCACCAAATAACACTGTCTC-BHQ; and MERS-sgRNA-rtR, GTAAGAGGGACTTTCCCGTGTTG. SSIII RT-PCR kit (Thermo Fisher Scientific) was used with 400 nM of each of the primers and 200 nM of the probe. Thermal cycling involved 10 min at 55°C for reverse transcription, followed by 3 min at 95°C and 45 cycles of 10 s at 95°C, 10 s at 56°C, and 20 s at 72°C. The products of sgRNA RT-PCR assay were analyzed on agarose gel, and tentative bands were sequenced.

MERS-CoV treatment with simulated gastrointestinal fluids

FaSSGF, FeSSGF, and FeSSIF powders (Biorelevant) were prepared into solutions according to the manufacturer's instruction. FaSSGF was additionally supplemented with pepsin (0.1 mg/ml; Sigma-Aldrich). A volume of 500 μl of MERS-CoV solution (7.5×10^6 PFU) was mixed with 5 ml of FaSSGF, FeSSIF, FeSSGF, or DMEM and then incubated at 37°C for the indicated minutes. An aliquot (1 ml) of the virus/fluid mixture was then sampled for virus titration in Vero-E6 cells after neutralization to pH 7.0 with 2.5 M sodium hydroxide. Human enterovirus EV71 and human coronavirus hCoV-229E were treated with the stimulated gastrointestinal fluids for comparison.

MERS-CoV infection in hDPP4 transgenic mice

First, nine female hDPP4 mice, 8 to 9 weeks old, were inoculated with 10^5 PFU of MERS-CoV (200 μl) via direct intragastric gavage. Three mice were administered with the proton pump inhibitor pantoprazole (40 mg/kg body weight) or PBS via intraperitoneal injection 2 hours before the virus challenge. At day 5 after virus inoculation, three pantoprazole-treated and three PBS-treated mice were sacrificed to harvest the lung and intestine for histopathological examination and viral load detection. Next, nine female hDPP4 mice were infected via intragastric gavage to characterize the early events after MERS-CoV inoculation. At days 1, 3, and 5 after intragastric gavage of MERS-CoV,

three mice were sacrificed to harvest the lung and intestine. To exclude the possible aspiration to the mouse airway during the intragastric gavage, 12 female mice, 6 of them pretreated with pantoprazole or mock-treated with PBS, were directly injected with 10^5 PFU of MERS-CoV (100 μl) into the mouse stomach after a 0.5-cm incision was made in the abdominal wall to expose the mouse stomach. Three pantoprazole- and PBS-treated mice were sacrificed at days 3 and 5 after infection. Mouse small intestine, lung, and brain were homogenized to detect live virus with plaque assay and quantify viral load with RT-qPCR. In each experiment, at least one mouse was inoculated with PBS as the mock infection control. The animal experiments were approved by the Institutional Animal Care and Use Committee of the Laboratory Animal Center, State Key Laboratory of Pathogen and Biosecurity, Beijing Institute of Microbiology and Epidemiology (BIME 2015-0025).

Immunofluorescence staining of the infected cells, intestinoids, and tissues

To identify virus-positive cells, cells on chamber slides and Transwell inserts, human intestinoids, slides of human small intestine, or mouse tissues were subjected to immunofluorescence staining, as described previously (*45*). Briefly, after permeabilization and blocking, cells, intestinoids, and tissues were stained with a guinea pig antiserum against MERS-CoV NP, followed with secondary antibodies including goat anti–guinea pig Alexa Fluor 488 immunoglobulin G (IgG) or goat anti–guinea pig Alexa Fluor 594 IgG (Abcam). For intestine explants and intestinoids, CK19 (YM3051, ImmunoWay), a marker of intestinal epithelial cell, was costained with an anti-NP antibody. To define the identity of the viral NP-positive cells in the tissues of infected hDPP4 mice, apart from the labeling of MERS-CoV NP, double staining was performed using a rat anti-mouse monoclonal CD68 antibody (FA-11, Abcam) and Alexa Fluor 568 goat anti-rat IgG (Life Technologies). After staining, intestinoids were whole-mounted with VECTASHIELD HardSet Antifade Mounting Medium (Vector Laboratories). The whole-mounted intestinoids, chamber slides, Transwell inserts, and tissue slides were imaged using a Carl Zeiss LSM 780 or 800 confocal microscope.

Flow cytometry analysis

MERS-CoV–infected human intestinoids and Transwell-cultured Caco-2 cells were digested into a single-cell suspension and fixed with 4% paraformaldehyde. MERS-CoV–positive cell was detected with the same MERS-CoV NP antiserum and goat anti–guinea pig Alexa Fluor 488 IgG, as described above. Active caspase-3 was detected with an Alexa Fluor 647–conjugated rabbit anti-human active caspase-3 antibody (BD Pharmingen). Cell permeabilization for intracellular staining was performed with 0.1% Triton X-100 in PBS. Immunostaining for flow cytometry was performed following standard procedures (*46*). The flow cytometry was performed using the FACSCanto II Analyzer (BD Biosciences), and data were analyzed using FlowJo vX (Tree Star).

Statistical analysis

Student's *t* test was used for data analysis. $P < 0.05$ was considered to be statistically significant.

SUPPLEMENTARY MATERIALS

Supplementary material for this article is available at http://advances.sciencemag.org/cgi/content/full/3/11/eaao4966/DC1

fig. S1. MERS-CoV replication in human primary intestinal epithelial cells.

fig. S2. Expression of human DPP4 on the surface of epithelial cells in intestinoids.

fig. S3. Formation of intact epithelial barrier in the polarized Caco-2 cells after Transwell culture.

fig. S4. The virus-positive cells in small intestine of an intragastrically inoculated mouse and those in the lung tissue of an intranasally inoculated mouse.

fig. S5. Identification of live viruses in the lung and brain homogenates and increased viral load in the brain tissues of intragastrically injected mice.

REFERENCES AND NOTES

1. A. M. Zaki, S. van Boheemen, T. M. Bestebroer, A. D. M. E. Osterhaus, R. A. M. Fouchier, Isolation of a novel coronavirus from a man with pneumonia in Saudi Arabia. *N. Engl. J. Med.* **367**, 1814–1820 (2012).
2. World Health Organization, *MERS-CoV Outbreak Update* (World Health Organization, 2017); www.who.int/emergencies/mers-cov/en/.
3. A. Assiri, J. A. Al-Tawfiq, A. A. Al-Rabeeah, F. A. Al-Rabiah, S. Al-Hajjar, A. Al-Barrak, H. Flemban, W. N. Al-Nassir, H. H. Balkhy, R. F. Al-Hakeem, H. Q. Makhdoom, A. I. Zumla, Z. A. Memish, Epidemiological, demographic, and clinical characteristics of 47 cases of Middle East respiratory syndrome coronavirus disease from Saudi Arabia: A descriptive study. *Lancet Infect. Dis.* **13**, 752–761 (2013).
4. J. F. W. Chan, S. K. P. Lau, K. K. W. To, V. C. C. Cheng, P. C. Y. Woo, K.-Y. Yuen, Middle East respiratory syndrome coronavirus: Another zoonotic betacoronavirus causing SARS-like disease. *Clin. Microbiol. Rev.* **28**, 465–522 (2015).
5. S. Cauchemez, P. Nouvellet, A. Cori, T. Jombart, T. Garske, H. Clapham, S. Moore, H. L. Mills, H. Salje, C. Collins, I. Rodriquez-Barraquer, S. Riley, S. Truelove, H. Algarni, R. Alhakeem, K. AlHarbi, A. Turkistani, R. J. Aguas, D. A. T. Cummings, M. D. Van Kerkhove, C. A. Donnelly, J. Lessler, C. Fraser, A. Al-Barrak, N. M. Ferguson, Unraveling the drivers of MERS-CoV transmission. *Proc. Natl. Acad. Sci. U.S.A.* **113**, 9081–9086 (2016).
6. D. R. Adney, N. van Doremalen, V. R. Brown, T. Bushmaker, D. Scott, E. de Wit, R. A. Bowen, V. J. Munster, Replication and shedding of MERS-CoV in upper respiratory tract of inoculated dromedary camels. *Emerg. Infect. Dis.* **20**, 1999–2005 (2014).
7. C. B. Reusken, E. A. Farag, M. Jonges, G. J. Godeke, A. M. El-Sayed, S. D. Pas, V. S. Raj, K. A. Mohran, H. A. Moussa, H. Ghobashy, F. Alhajri, A. K. Ibrahim, B. J. Bosch, S. K. Pasha, H. E. Al-Romaihi, M. Al-Thani, S. A. Al-Marri, M. M. AlHajri, B. L. Haagmans, M. P. Koopmans, Middle East respiratory syndrome coronavirus (MERS-CoV) RNA and neutralising antibodies in milk collected according to local customs from dromedary camels, Qatar, April 2014. *Euro. Surveill.* **19**, 20829 (2014).
8. N. van Doremalen, T. Bushmaker, W. B. Karesh, V. J. Munster, Stability of Middle East respiratory syndrome coronavirus in milk. *Emerg. Infect. Dis.* **20**, 1263–1264 (2014).
9. Z. A. Memish, M. Cotten, B. Meyer, S. J. Watson, A. J. Alsahafi, A. A. Al Rabeeah, V. M. Corman, A. Sieberg, H. Q. Makhdoom, A. Assiri, M. Al Masri, S. Aldabbagh, B.-J. Bosch, M. Beer, M. A. Müller, P. Kellam, C. Drosten, Human infection with MERS coronavirus after exposure to infected camels, Saudi Arabia, 2013. *Emerg. Infect. Dis.* **20**, 1012–1015 (2014).
10. P. Durai, M. Batool, M. Shah, S. Choi, Middle East respiratory syndrome coronavirus: Transmission, virology and therapeutic targeting to aid in outbreak control. *Exp. Mol. Med.* **47**, e181 (2015).
11. J. A. Al-Tawfiq, Z. A. Memish, Middle East respiratory syndrome coronavirus: Epidemiology and disease control measures. *Infect. Drug Resist.* **7**, 281–287 (2014).
12. S. S. Lee, N. S. Wong, Probable transmission chains of Middle East respiratory syndrome coronavirus and the multiple generations of secondary infection in South Korea. *Int. J. Infect. Dis.* **38**, 65–67 (2015).
13. N. van Doremalen, T. Bushmaker, V. J. Munster, Stability of Middle East respiratory syndrome coronavirus (MERS-CoV) under different environmental conditions. *Euro. Surveill.* **18**, 20590 (2013).
14. S. Y. Bin, J. Y. Heo, M.-S. Song, J. Lee, E.-H. Kim, S. J. Park, H. I. Kwon, S. M. Kim, Y.-i. Kim, Y.-J. Si, I.-W. Lee, Y. H. Baek, W.-S. Choi, J. Min, H. W. Jeong, Y. K. Choi, Environmental contamination and viral shedding in MERS patients during MERS-CoV outbreak in South Korea. *Clin. Infect. Dis.* **62**, 755–760 (2016).
15. G. K.-M. Goh, A. K. Dunker, V. N. Uversky, Understanding viral transmission behavior via protein intrinsic disorder prediction: Coronaviruses. *J. Pathog.* **2012**, 738590 (2012).
16. G. K.-M. Goh, A. K. Dunker, V. Uversky, Prediction of intrinsic disorder in MERS-CoV/HCoV-EMC supports a high oral-fecal transmission. *PLOS Curr.* **5** (2013).
17. V. M. Corman, A. M. Albarrak, A. S. Omrani, M. M. Albarrak, M. E. Farah, M. Almasri, D. Muth, A. Sieberg, B. Meyer, A. M. Assiri, T. Binger, K. Steinhagen, E. Lattwein, J. Al-Tawfiq, M. A. Müller, C. Drosten, Z. A. Memish, Viral shedding and antibody response in 37 patients with Middle East respiratory syndrome coronavirus infection. *Clin. Infect. Dis.* **62**, 477–483 (2016).
18. T. Sato, D. E. Stange, M. Ferrante, R. G. Vries, J. H. Van Es, S. Van den Brink, W. J. Van Houdt, A. Pronk, J. Van Gorp, P. D. Siersema, H. Clevers, Long-term expansion of epithelial organoids from human colon, adenoma, adenocarcinoma, and Barrett's epithelium. *Gastroenterology* **141**, 1762–1772 (2011).

19. K. Wang, S. T. Yuen, J. Xu, S. P. Lee, H. H. N. Yan, S. T. Shi, H. C. Siu, S. Deng, K. M. Chu, S. Law, K. H. Chan, A. S. Chan, W. Y. Tsui, S. L. Ho, A. K. W. Chan, J. L. K. Man, V. Foglizzo, M. K. Ng, A. S. Chan, Y. P. Ching, G. H. W. Cheng, T. Xie, J. Fernandez, V. S. W. Li, H. Clevers, P. A. Rejto, M. Mao, S. Y. Leung, Whole-genome sequencing and comprehensive molecular profiling identify new driver mutations in gastric cancer. *Nat. Genet.* **46**, 573–582 (2014).
20. Y. Yin, M. Bijvelds, W. Dang, L. Xu, A. A. van der Eijk, K. Knipping, N. Tuysuz, J. F. Dekkers, Y. Wang, J. de Jonge, D. Sprengers, L. J. van der Laan, J. M. Beekman, D. Ten Berge, H. J. Metselaar, H. de Jonge, M. P. Koopmans, M. P. Peppelenbosch, Q. Pan, Modeling rotavirus infection and antiviral therapy using primary intestinal organoids. *Antiviral Res.* **123**, 120–131 (2015).
21. S. R. Finkbeiner, X.-L. Zeng, B. Utama, R. L. Atmar, N. F. Shroyer, M. K. Estes, Stem cell-derived human intestinal organoids as an infection model for rotaviruses. *MBio* **3**, e00159-12 (2012).
22. A. L. Kauffman, A. V. Gyurdieva, J. R. Mabus, C. Ferguson, Z. Yan, P. J. Hornby, Alternative functional in vitro models of human intestinal epithelia. *Front. Pharmacol.* **4**, 79 (2013).
23. G. Zhao, Y. Jiang, H. Qiu, T. Gao, Y. Zeng, Y. Guo, H. Yu, J. Li, Z. Kou, L. Du, W. Tan, S. Jiang, S. Sun, Y. Zhou, Multi-organ damage in human dipeptidyl peptidase 4 transgenic mice infected with Middle East respiratory syndrome-coronavirus. *PLOS ONE* **10**, e0145561 (2015).
24. X. Tao, T. Garron, A. S. Agrawal, A. Algaissi, B.-H. Peng, M. Wakamiya, T.-S. Chan, L. Lu, L. Du, S. Jiang, R. B. Couch, C.-T. Tseng, Characterization and demonstration of the value of a lethal mouse model of Middle East respiratory syndrome coronavirus infection and disease. *J. Virol.* **90**, 57–67 (2015).
25. K. Li, C. Wohlford-Lenane, S. Perlman, J. Zhao, A. K. Jewell, L. R. Reznikov, K. N. Gibson-Corley, D. K. Meyerholz, P. B. McCray Jr., Middle East respiratory syndrome coronavirus causes multiple organ damage and lethal disease in mice transgenic for human dipeptidyl peptidase 4. *J. Infect. Dis.* **213**, 712–722 (2016).
26. P. Gautret, G. C. Gray, R. N. Charrel, N. G. Odezulu, J. A. Al-Tawfiq, A. Zumla, Z. A. Memish, Emerging viral respiratory tract infections—Environmental risk factors and transmission. *Lancet Infect. Dis.* **14**, 1113–1122 (2014).
27. F. Zielecki, M. Weber, M. Eickmann, L. Spiegelberg, A. M. Zaki, M. Matrosovich, S. Becker, F. Weber, Human cell tropism and innate immune system interactions of human respiratory coronavirus EMC compared to those of severe acute respiratory syndrome coronavirus. *J. Virol.* **87**, 5300–5304 (2013).
28. R. W. Y. Chan, M. C. W. Chan, S. Agnihothram, L. L. Y. Chan, D. I. T. Kuok, J. H. M. Fong, Y. Guan, L. L. M. Poon, R. S. Baric, J. M. Nicholls, J. S. M. Peiris, Tropism of and innate immune responses to the novel human betacoronavirus lineage C virus in human ex vivo respiratory organ cultures. *J. Virol.* **87**, 6604–6614 (2013).
29. J. Zhou, H. Chu, J. F.-W. Chan, K.-Y. Yuen, Middle East respiratory syndrome coronavirus infection: Virus-host cell interactions and implications on pathogenesis. *Virol. J.* **12**, 218 (2015).
30. P. J. Quin, B. K. Markey, F. C. Leonard, E. S. Fitzpatrick, S. Fanning, P. Hartigan, *Veterinary Microbiology and Microbial Disease* (Wiley-Blackwell, ed. 2, 2011).
31. C. Weiss, H. F. Clark, Rapid inactivation of rotaviruses by exposure to acid buffer or acidic gastric juice. *J. Gen. Virol.* **66** (Pt. 12), 2725–2730 (1985).
32. A. Assiri, A. McGeer, T. M. Perl, C. S. Price, A. A. Al Rabeeah, D. A. T. Cummings, Z. N. Alabdullatif, M. Assad, A. Almulhim, H. Makhdoom, H. Madani, R. Alhakeem, J. A. Al-Tawfiq, M. Cotten, S. J. Watson, P. Kellam, A. I. Zumla, Z. A. Memish; KSA MERS-CoV Investigation Team, Hospital outbreak of Middle East respiratory syndrome coronavirus. *N. Engl. J. Med.* **369**, 407–416 (2013).
33. Z. A. Memish, A. I. Zumla, R. F. Al-Hakeem, A. A. Al-Rabeeah, G. M. Stephens, Family cluster of Middle East respiratory syndrome coronavirus infections. *N. Engl. J. Med.* **368**, 2487–2494 (2013).
34. A. Mailles, K. Blanckaert, P. Chaud, S. van der Werf, B. Lina, V. Caro, C. Campese, B. Guéry, H. Prouvost, X. Lemaire, M. C. Paty, S. Haeghebaert, D. Antoine, N. Ettahar, H. Noel, S. Behillil, S. Hendricx, J. C. Manuguerra, V. Enouf, G. La Ruche, C. Semaille, B. Coignard, D. Lévy-Bruhl, F. Weber, C. Saura, D. Che; Collective The investigation team, First cases of Middle East respiratory syndrome coronavirus (MERS-CoV) infections in France, investigations and implications for the prevention of human-to-human transmission, France, May 2013. *Euro. Surveill.* **18**, 20502 (2013).
35. K. Shinya, A. Makino, H. Tanaka, M. Hatta, T. Watanabe, M. Q. Le, H. Imai, Y. Kawaoka, Systemic dissemination of H5N1 influenza A viruses in ferrets and hamsters after direct intragastric inoculation. *J. Virol.* **85**, 4673–4678 (2011).
36. A. Martin, S. M. Lemon, Hepatitis A virus: From discovery to vaccines. *Hepatology* **43**, S164–S172 (2006).
37. A. Vabret, T. Mourez, S. Gouarin, J. Petitjean, F. Freymuth, An outbreak of coronavirus OC43 respiratory infection in Normandy, France. *Clin. Infect. Dis.* **36**, 985–989 (2003).
38. J. S. M. Peiris, S. T. Lai, L. L. M. Poon, Y. Guan, L. Y. C. Yam, W. Lim, J. Nicholls, W. K. S. Yee, W. W. Yan, M. T. Cheung, V. C. C. Cheng, K. H. Chan, D. N. C. Tsang, R. W. H. Yung, T. K. Ng, K. Y. Yuen: SARS study group, Coronavirus as a possible cause of severe acute respiratory syndrome. *Lancet* **361**, 1319–1325 (2003).
39. W. K. Leung, K.-f. To, P. K. S. Chan, H. L. Y. Chan, A. K. L. Wu, N. Lee, K. Y. Yuen, J. J. Y. Sung, Enteric involvement of severe acute respiratory syndrome-associated coronavirus infection. *Gastroenterology* **125**, 1011–1017 (2003).
40. I. F. N. Hung, V. C. C. Cheng, A. K. L. Wu, B. S. F. Tang, K. H. Chan, C. M. Chu, M. M. L. Wong, W. T. Hui, L. L. M. Poon, D. M. W. Tse, K. S. Chan, P. C. Y. Woo, S. K. P. Lau, J. S. M. Peiris, K. Y. Yuen, Viral loads in clinical specimens and SARS manifestations. *Emerg. Infect. Dis.* **10**, 1550–1557 (2004).
41. Y. Ding, L. He, Q. Zhang, Z. Huang, X. Che, J. Hou, H. Wang, H. Shen, L. Qiu, Z. Li, J. Geng, J. Cai, H. Han, X. Li, W. Kang, D. Weng, P. Liang, S. Jiang, Organ distribution of severe acute respiratory syndrome (SARS) associated coronavirus (SARS-CoV) in SARS patients: Implications for pathogenesis and virus transmission pathways. *J. Pathol.* **203**, 622–630 (2004).
42. P. J. Openshaw, Crossing barriers: Infections of the lung and the gut. *Mucosal Immunol.* **2**, 100–102 (2009).
43. L. J. Saif, Bovine respiratory coronavirus. *Vet. Clin. North Am. Food Anim. Pract.* **26**, 349–364 (2010).
44. J. Zhou, H. Chu, C. Li, B. H.-Y. Wong, Z.-S. Cheng, V. K.-M. Poon, T. Sun, C. C.-Y. Lau, K.-K. Wong, J. Y.-W. Chan, J. F.-W. Chan, K. K.-W. To, K.-H. Chan, B.-J. Zheng, K.-Y. Yuen, Active replication of Middle East respiratory syndrome coronavirus and aberrant induction of inflammatory cytokines and chemokines in human macrophages: Implications for pathogenesis. *J. Infect. Dis.* **209**, 1331–1342 (2014).
45. J. Zhou, T. Tan, Y. Tian, B. Zheng, J.-H. Ou, E. J. Huang, T. S. B. Yen, Krüppel-like factor 15 activates hepatitis B virus gene expression and replication. *Hepatology* **54**, 109–121 (2011).
46. H. Chu, J. Zhou, B. H.-Y. Wong, C. Li, J. F.-W. Chan, Z.-S. Cheng, D. Yang, D. Wang, A. C.-Y. Lee, C. Li, M.-L. Yeung, J.-P. Cai, I. H.-Y. Chan, W.-K. Ho, K.-K. To, B.-J. Zheng, Y. Yao, C. Qin, K.-Y. Yuen, Middle East respiratory syndrome coronavirus efficiently infects human primary T lymphocytes and activates the extrinsic and intrinsic apoptosis pathways. *J. Infect. Dis.* **213**, 904–914 (2016).

Acknowledgments: We thank H. Clevers (Hubrecht Institute) for providing the reagents for organoid cultures. We also thank C. C. Y. Yip, J.-P. Cai, and Faculty Core Facility (Li Ka Shing Faculty of Medicine, University of Hong Kong) for technical assistance. **Funding:** The study is partly supported by the Health and Medical Research Fund (reference nos.14131392 and 15140762) of Food and Health Bureau; the National Natural Science Foundation of China/ Research Grants Council Joint Research Scheme (N_HKU728/14); the Collaborative Research Fund (C7011-15R) of the Research Grants Council; the Theme-Based Research Scheme (T11/707/15) of the Research Grants Council, Hong Kong Special Administrative Region; Collaborative Innovation Center for Diagnosis and Treatment of Infectious Diseases, Ministry of Education of China; the National Project of Infectious Disease (2014ZX10004001004), Ministry of Science and Technology of China; the German Research Foundation (Deutsche Forschungsgemeinschaft grants DR772/12-1 and DR772/7-2); and the European Commission project PREPARE (contract number 602525). **Author contributions:** J.Z. and K.-Y.Y. designed the study. J.Z., C.L., H.C., D.W., V.K.-M.P., B.H.-Y.W., X.Z., M.C.C., D.Y., and Y.W. performed the in vitro experiments. H.H.-N.Y. and S.Y.L. provided the intestinal organoids. G.Z. and S.S. performed the animal experiments. J.Z., C.L., H.C., D.W., L.W., J.F.-W.C., K.K.-W.T., and I.F.-N.H. analyzed and interpreted the data. R.K.H.A.-Y. reviewed histopathology. I.H.-Y.C. provided the normal human intestine. Z.A.M., V.M.C., and C.D. examined the specimens of MERS patients. Y.Z. provided the hDPP4 mice. J.Z., H.C., J.F.-W.C., K.K.-W.T., and K.-Y.Y. wrote and revised the manuscript. **Competing interests:** S.Y.L. has received research sponsorship from Pfizer, Merck, and Servier. The sponsors were not involved in the study design, data collection, and analysis. The other authors declare that they have no competing interests. **Data and materials availability:** All data needed to evaluate the conclusions in the paper are present in the paper and/or the Supplementary Materials. Additional data related to this paper may be requested from the authors.

Submitted 27 July 2017
Accepted 20 October 2017
Published 15 November 2017
10.1126/sciadv.aao4966

Citation: J. Zhou, C. Li, G. Zhao, H. Chu, D. Wang, H. H.-N. Yan, V. K.-M. Poon, L. Wen, B. H.-Y. Wong, X. Zhao, M. C. Chiu, D. Yang, Y. Wang, R. K. H. Au-Yeung, I. H.-Y. Chan, S. Sun, J. F.-W. Chan, K. K.-W. To, Z. A. Memish, V. M. Corman, C. Drosten, I. F.-N. Hung, Y. Zhou, S. Y. Leung, K.-Y. Yuen, Human intestinal tract serves as an alternative infection route for Middle East respiratory syndrome coronavirus. *Sci. Adv.* **3**, eaao4966 (2017).